Article ID: 1000-324X(2021)11-1223-08 **DOI:** 10.15541/jim20210142

Ultrafast CO Sensor Based on Flame-annealed Porous CeO_2 Nanosheets for Environmental Application

LI Pengpeng, WANG Bing, WANG Yingde

(Science and Technology on Advanced Ceramic Fibers and Composites Laboratory, College of Aerospace Science and Engineering, National University of Defense Technology, Changsha 410073, China)

Abstract: As a highly toxic gas, CO is one of the culprits of air pollution. Long-term inhalation will also cause great harm to the human body and even death. How to achieve rapid CO monitoring is an important challenge in sensing field. CO as one of the of air pollution, long time inhalation will reduce the oxygen carrying capacity of blood and in severe cases death. Therefore, effective monitoring of CO is necessary. In this study, porous CeO_2 nanosheets (CeO_2 NSs) were obtained *via* flame annealing intermediate product $CeCO_3OH$ nanosheets synthesized by simple hydrothermal method. Through controlling of the flame time, oxygen vacancies were introduced into the CeO_2 NSs. As a result, the CeO_2 NSs annealed with 2 min (CeO_2-2min NSs) exhibited outstanding reproducibility and selectivity towards CO gas. Particularly, the response/recovery time were extremely fast (2 s/2 s) towards 500 μL/L CO at 450 ℃ as well as finely functional relationship between response and concentration of CO at a wide detection range (10–10000 μL/L). The superior gas sensing performance of CeO_2-2min NSs can be ascribed to the high aspect ratios of the porous two-dimensional structure and abundant oxygen vacancies in the crystals. This work may supply a strategy for designing ultrafast gas sensors which can detect target gas at a wide range.

Key words: flame annealing; porous CeO_2 nanosheets; oxygen vacancy; gas sensors; wide range

Carbon monoxide (CO) which is colorless, odorless, but toxic, explosive, mainly produced by automotive emissions, coal combustion and forest fires *etc*.[1] Actually, any incomplete combustion of carbon could generate CO. However, CO is extremely harmful to human beings causing dizziness, nausea or even death[2]. According to the data from World Health Organization, one can tolerate 9 μL/L CO within 8 h, 26 μL/L within 1 h, and beyond this the gas could threaten human life[3]. As a result, there are various CO gas sensors to monitor CO. However, to the best of our knowledge, the detection ranges of these CO gas sensors are limited. Therefore, developing CO gas sensors with a wide detection range becomes a crucially important task.

Many materials could be used to detect CO gas[4]. Taking flexibility and versatility in practical applications into account, metal oxides are promising sensing materials for CO gas sensors[5]. Specifically, SnO_2, ZnO, Co_3O_4 and TiO_2 *etc*. have been reported as CO gas sensors, which exhibit a detection range from dozens of μL/L to thousands of μL/L[6-7]. Among them, cerium oxide (CeO_2), featured of structural stability and high redox capability[8], has been extensively investigated in gas sensing field[9]. Good CO sensing performance was obtained by pristine CeO_2 nanospheres with high surface area and the detection range was 10–30 μL/L[10]. SnO_2 mixed CeO_2 thin films exhibited a response/recovery time of 26 s/30 s towards 500 μL/L CO and the detection concentration was in the range of 5–5000 μL/L[11]. Although various CeO_2, such as samples with different morphologies, mixture of other metal oxides or precious metals, has been reported, the detection range of these CO sensors are not wide enough as well as dozens of seconds of response time to meet practical requirements in some cases.

Two-dimensional nanosheets exhibit superiority in specific surface area, mobility of ions and the number of active sites, being applied in many aspects[12]. In the context of gas sensing, two-dimensional nanosheets also show remarkable performance. For instance, Liu *et al*.[13] synthesized porous ultrathin ZnO nanosheets with high

Received date: 2021-03-10; **Revised date:** 2021-04-10; **Published online:** 2021-04-30
Foundation item: National Natural Science Foundation of China (61701514, 51773226); Natural Science Foundation of Hunan Province (2018JJ3603)
Biography: LI Pengpeng(1995–), male, Master candidate. E-mail: lipengpeng@nudt.edu.cn
李鹏鹏(1995–), 男, 硕士研究生. E-mail: lipengpeng@nudt.edu.cn
Corresponding author: WANG Yingde, professor. E-mail: wangyingde@nudt.edu.cn;WANG Bing, associate professor. E-mail: bingwang@nudt.edu.cn
王应德, 教授. E-mail: wangyingde@nudt.edu.cn; 王 兵, 副研究员. E-mail: bingwang@nudt.edu.cn

specific surface areas for acetylacetone gas sensing and presented significant results, demonstrating the important role of oxygen vacancies in gas sensing spontaneously. Self-assembled monolayer CuO nanosheets were used for H_2S gas sensing with improved sensitivity[14]. Selective alkene gas sensing was achieved by SnO_2 nanosheets with distinct performance, which is affected by the content of oxygen vacancies[15]. However, to the best of our knowledge, there is almost few reports about CeO_2 NSs, especially for the influence of oxygen vacancies of CeO_2 NSs on the sensing performance.

In this study, we prepared CeO_2 NSs *via* flame annealing under different time intermediate product $CeCO_3OH$ nanosheets synthesized by simple hydrothermal method. The as-prepared samples were characterized by various methods. These flame-annealed CeO_2 NSs show ultrafast response/recovery time towards CO, wide-range CO detection as well as good reproducibility and selectivity. Moreover, the mechanism of CO gas sensing is discussed.

1 Experimental

1.1 Materials

Cerium (Ⅲ) chloride heptahydrate ($CeCl_3·7H_2O$) and sodium oleate were purchased from Shanghai Macklin Biochemical Co., Ltd. Ammonium hydroxide ($NH_3·H_2O$) and cyclohexane were provided by Sinopharm Chemical Reagent Co., Ltd. All of the chemicals and solvents were reagent-grade without further purification. Deionized water was used in all procedure.

1.2 Synthesis of CeO_2 nanosheets

Intermediate product $CeCO_3OH$ was synthesized by a simple hydrothermal method according to our previous work[16] as shown in Fig.1. The specific procedure was listed as follows. $CeCl_3·7H_2O$ solution was dropped into sodium oleate solution with stirring. After that, $NH_3·H_2O$ was dropped into it with stirring. Subsequently, the suspension was proceeded with hydrothermal reaction. The precipitant was collected by centrifugation and washed with cyclohexane. Whereafter, the intermediate product was annealed with liquefied butane gas flame for 0.5, 2, 5 min and the resulted CeO_2 nanosheets were denoted as CeO_2-0.5min NSs, CeO_2-2min NSs, and CeO_2-5min NSs, respectively (The flame temperature is in the range of 1000–1200 ℃). The samples were collected for further characterization.

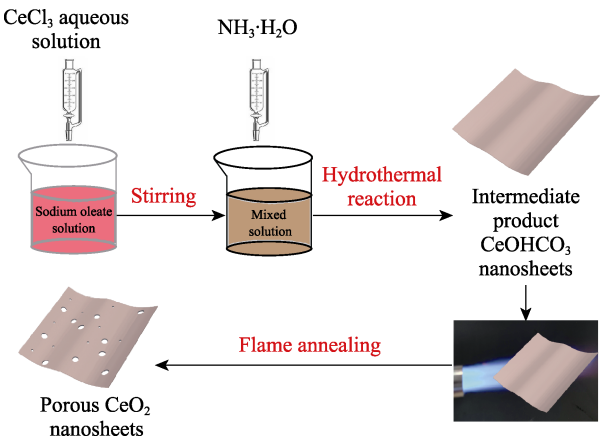

Fig. 1 Schematic illustration of preparation of CeO_2 nanosheets

1.3 Characterization

The crystal structure was confirmed by X-ray Diffraction (XRD, Bruker AXS D8 Advanced Diffractometer, German) with Cu Kα radiation (λ=0.15418 nm). The morphology and structures were characterized *via* transmission electron microscope (TEM, Tian G2 60-300, FEI, USA). The element compositions and chemical states were obtained by X-ray photoelectron spectroscope (XPS, Thermo Scientific Escalab 250Xi, USA) equipped with a monochromatic Al Kα source. The specific surface area and porosity were evaluated using an automated surface area and pore size analyzer (Quantachrome Autosorb iQ3, USA), calculated by Brunauer-Emmett-Teller (BET) and Barrett-Joyner-Halenda (BJH) methods on the basis of nitrogen adsorption-desorption isotherms, respectively. The presence of oxygen vacancies was determined using electron paramagnetic resonance (EPR, Bruker A300, German).

1.4 Gas sensing test

Specialized CGS-1 TP intelligent gas sensing analyzing system (Beijing Elite Tech Co., Ltd, Beijing, China) was adopted in this work and the fabrication detail and testing principal could be found in our previous report[17]. The gas sensing response (S) was defined as the following formula:

$$S = \frac{|R_a - R_g|}{R_a} \times 100\% \quad (1)$$

where R_a and R_g represent the resistance of sensing materials in air and target gas, respectively. The response and recovery time were labelled as the time to reach 90% of the total resistance change.

2 Results and discussion

2.1 Characterization

In order to identity the crystal structure, the intermediate product and the as-prepared CeO_2 nanosheets were carefully investigated by XRD. The patterns of intermediate product perfectly matches with $CeCO_3OH$ (JCPDF 32-0189) as shown in Fig. S1. XRD patterns of CeO_2-0.5min NSs, CeO_2-2min NSs and CeO_2-5min NSs show sharp diffraction peaks, which demonstrates high cry-

stallinity as shown in Fig. 2. These diffraction peaks can be well indexed to cubic fluorite cerium oxide (JCPDF 34-0394). The typical peaks located at 2θ=28.6°, 33.0°, 47.5°, 56.3°, 59.1°, 69.4°, 76.7°, 79.0°, correspond to (111), (200), (220), (311), (222), (400), (331), (420) crystal planes of fluorite phase of CeO_2, respectively. However, the width of main diffraction peak of (111) at 2θ=28.6° is quite different. With flame annealing time increasing, the diffraction peak width become narrower, demonstrating the increment of crystal sizes. The crystal sizes based on (111) crystal plane of CeO_2-0.5min NSs, CeO_2-2min NSs and CeO_2-5min NSs were calculated to be 12.12, 17.02 and 20.32 nm, respectively, according to the Scherer equation.

The element compositions and surface chemical states could be detected by XPS, and the details are given in Fig. 3. For O element, the O1s core level spectra of CeO_2-0.5min NSs, CeO_2-2min NSs and CeO_2-5min NSs can be deconvolved into three peaks, *i.e.* lattice oxygen (O_L, *ca.* 529.0 eV), deficient oxygen (O_V, *ca.* 529.5 eV) and sorbed oxygen (O_S, *ca.* 531.2 eV) in Fig. 3(a, b, c), respectively[18]. As is well-known, O_V and O_S (O_2^-, O^- or O^{2-}) play absolutely important roles in gas sensing, contributing to improving response[19]. Table S1 provides the ratio of each oxygen species to the whole oxygen extent. In this study, CeO_2-2min NSs possesses the largest amount of O_V (43.2%), and these for CeO_2-0.5min NSs and CeO_2-5min NSs are relatively smaller. For Ce element, the Ce3d core level spectra of CeO_2-0.5min NSs, CeO_2-2min NSs and CeO_2-5min NSs can be deconvolved into ten peaks in Fig. 3(d, e, f), respectively. The peaks at about 916.4, 907.1, 902.4 and 900.5 eV are designated to $Ce3d_{3/2}$, and that at about 898.2, 897.8, 888.5, 884.5, 882.1 and 881.4 eV pertain to $Ce3d_{5/2}$[20]. Thereinto, the peaks at about 881.4, 884.5, 897.8 and 902.4 eV are assigned to Ce^{3+}, and those at around 882.1, 888.5, 898.2, 900.5, 907.1 and 916.4 eV belong to Ce^{4+}[21]. Moreover, the ratio of Ce^{3+} to the total extent of Ce is presented in Table S1. It was reported that there is a transformation between Ce^{4+} and Ce^{3+} which determines by the oxygen partial pressure. That means that with more Ce^{3+}, more O_V exists in the samples[8]. In this case, CeO_2-2min NSs holds the largest part of Ce^{3+} (28.6%), consistently with the largest part of O_V (43.2%).

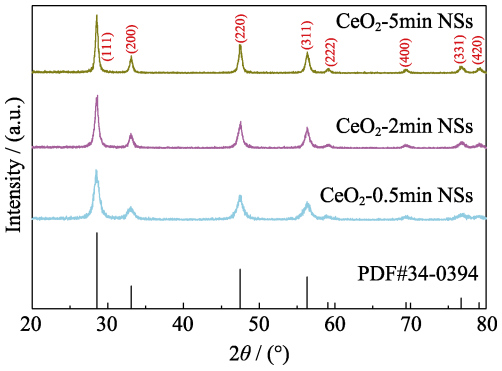

Fig. 2　XRD patterns of the flame-annealed CeO_2 nanosheets

The morphology and structure were characterized by TEM. The spectra of CeO_2-0.5min NSs, CeO_2-2min NSs and CeO_2-5min NSs are given in Fig. 4(a, b, c), respectively, which are transparent nanosheets with pores (labelled by

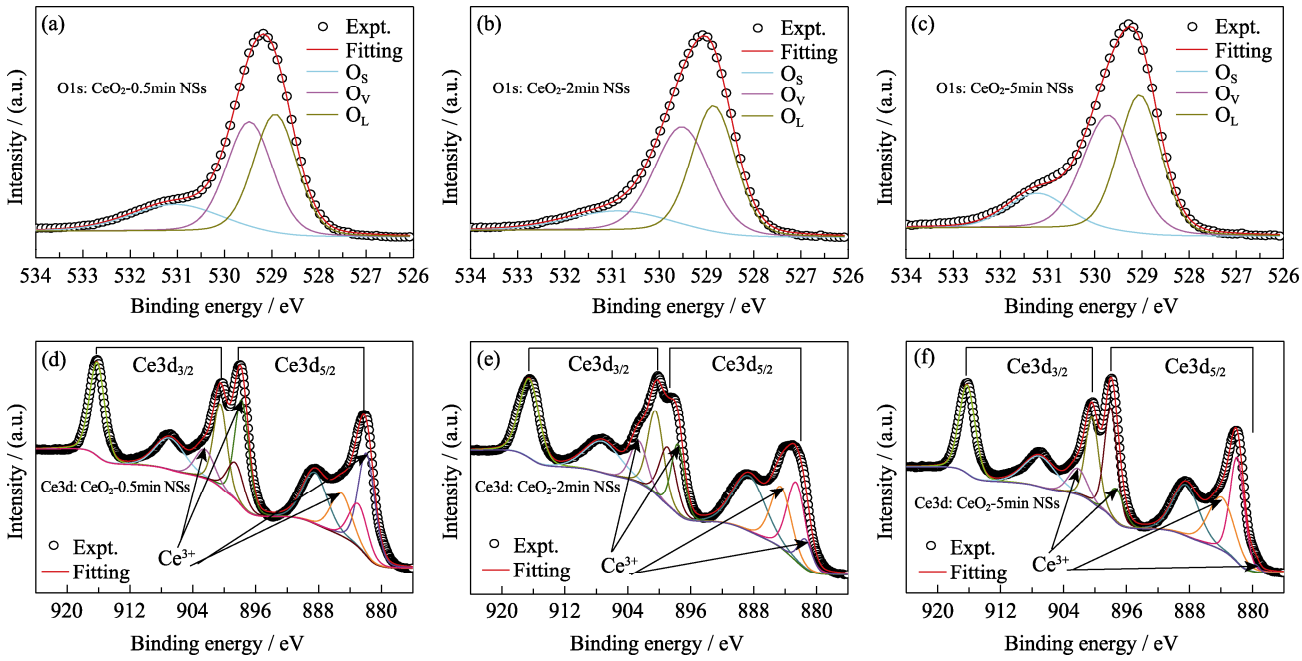

Fig. 3　XPS spectra of the CeO_2 NSs

(a, b, c) high resolution spectra of O 1s of CeO_2-0.5min NSs, CeO_2-2min NSs and CeO_2-5min NSs;

(d, e, f) high resolution spectra of Ce 3d of CeO_2-0.5min NSs, CeO_2-2min NSs and CeO_2-5min NSs

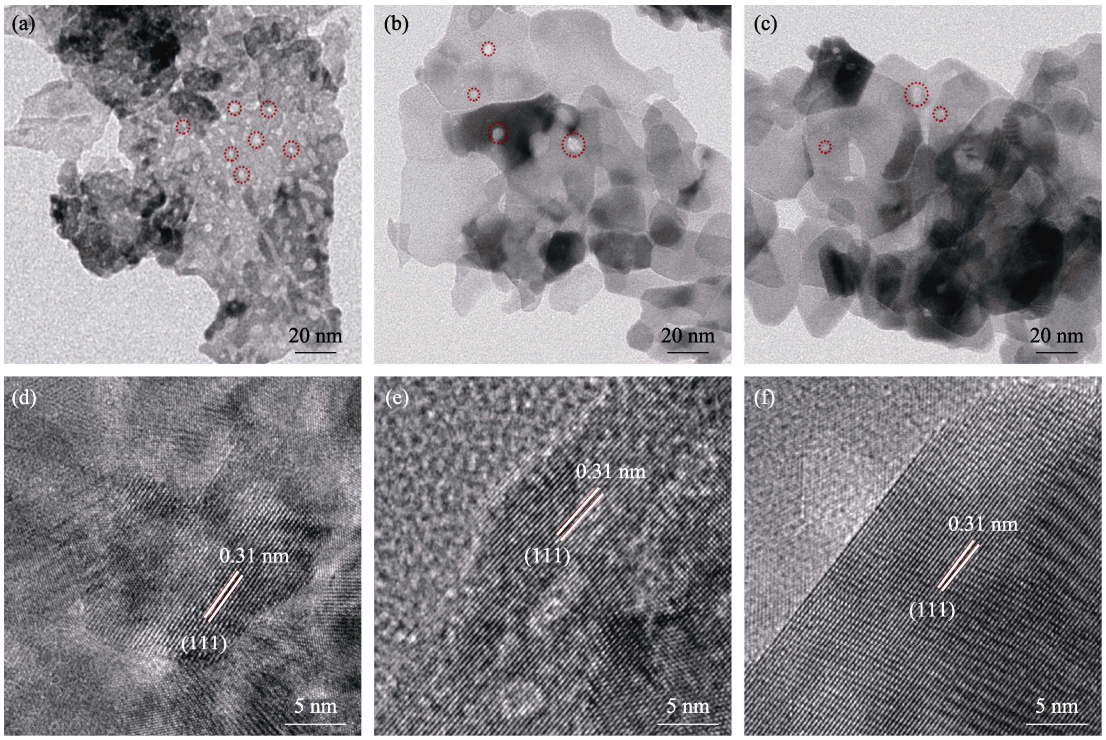

Fig. 4 Morphologies and structure characterizations of the as-prepared samples
(a, b, c) TEM images of CeO_2-0.5min NSs, CeO_2-2min NSs and CeO_2-5min NSs (pores are labelled by red dotted circles);
(d, e, f) HRTEM images of CeO_2-0.5min NSs, CeO_2-2min NSs and CeO_2-5min NSs

red dotted circles). Nevertheless, there is a difference in pore diameters that with the increase of flame time, the pore diameter becomes larger. This result is consistent with the tendency of nitrogen adsorption-desorption discussed later, which may influence the gas sensing performance. More importantly, with the increment of flame annealing time, the grain sizes become larger, which is consistent with the results of XRD. The crystal structure and crystal lattice spacing of the samples can be observed by HRTEM, as shown in Fig. 4(d,e,f), respectively. The distance of two adjacent crystal planes is 0.31 nm, corresponding to (111) planes of the CeO_2 fluorite phase. Obviously, crystallinity increases along with a longer flame annealing time.

Nitrogen adsorption-desorption isothermal curves were performed to characterize the aspect surface area and porosity of the samples, as shown in Fig. 5. It is observed from Fig. 5(a) that all samples exhibit the isotherm feature of the IV-type with a hysteresis loop according to the IUPAC classification, which indicates the existence of a mesoporous structure in nanosheets[22]. The surface area of CeO_2-0.5min NSs, CeO_2-2min NSs and CeO_2-5min NSs are 73.344, 46.804 and 40.836 $m^2 \cdot g^{-1}$, respectively, summarized in Table S2. It is noticed that with the flame annealing time increasing, the surface area becomes smaller, which may be contributed to congregation and growth of small grains during the annealing process. Nevertheless, there is a variance in pore size distribution.

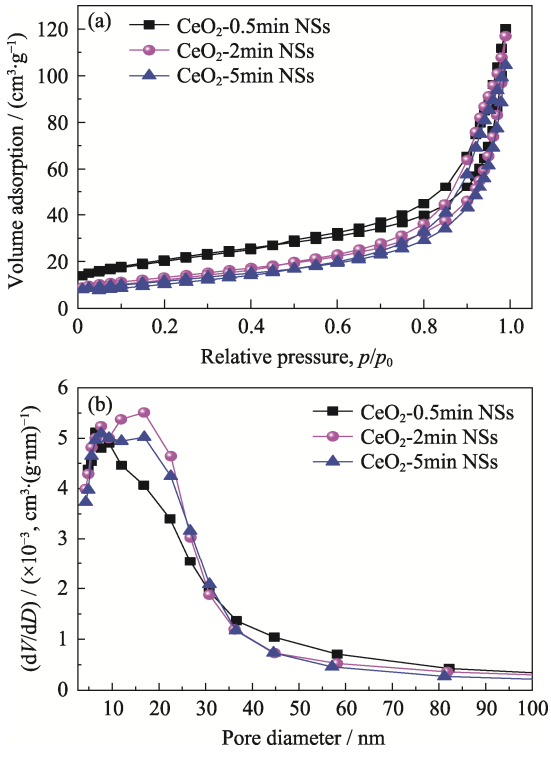

Fig. 5 (a) Nitrogen adsorption-desorption isotherms and (b) pore size distributions of CeO_2 NSs

As shown in Fig. 5(b), CeO_2-2min NSs (15.5 nm) and CeO_2-5min NSs (15.8 nm) possess larger pore diameter than CeO_2-0.5min NSs (10.1 nm), which indicates gas molecules easily adsorb and desorb on the surface of

CeO_2-2min NSs and CeO_2-5min NSs as well as a fast response/recovery time.

To further verify the presence of oxygen vacancies, EPR were performed to ascertain relative amount of oxygen vacancies in each sample, as shown in Fig. 6. The value of *g* represents different species which contain unpaired electron. In this case, all samples have the same value of *g*(2.0038), which typically demonstrates the presence of oxygen vacancies in the samples[19]. The intensity of CeO_2-2min NSs and CeO_2-5min NSs is almost identical and far larger than that for CeO_2-0.5min NSs, which confirms that oxygen vacancies in CeO_2-2min NSs and CeO_2-5min NSs are abundant and much higher than that in CeO_2-0.5min NSs, consistent with the results of XPS.

2.2 Gas sensing properties

We systematically investigated the gas sensing performances of the samples, as shown in Fig. 7. First of all, the response of the sensors towards 500 μL/L CO were measured from 300 ℃ to 500 ℃ with the interval of 50 ℃ to determine the optimal temperature. For CeO_2-2min NSs and CeO_2-5min NSs, the optimal temperature is 450 ℃, and that for CeO_2-0.5min NSs is 400 ℃ in Fig. 7(a). However, the responses of CeO_2-2min NSs (10%) and CeO_2-5min NSs (9%) are far higher than that for CeO_2-0.5min NSs (4%). The responses of CeO_2-2min NSs and CeO_2-5min NSs are considerable, which may be ascribed to the comparable O_V content demonstrated by XPS (Table S1, 43.2% and 42.7%, respectively) and EPR (Fig. 6). For a little higher response of CeO_2-2min NSs than CeO_2-5min NSs, the difference between surface area (Table S2) and the content of Ce^{3+} (Table S1) may account for it. However, there is a large gap between the response of CeO_2-2min NSs and CeO_2-0.5min NSs, which may be resulted from the discrepancy of the amount of O_V (Table S1 and Fig. 6) and pore diameters (Fig. 5(b)). Therefore, CeO_2-2min NSs was chosen to proceed further testing at its optimal temperature(450 ℃).

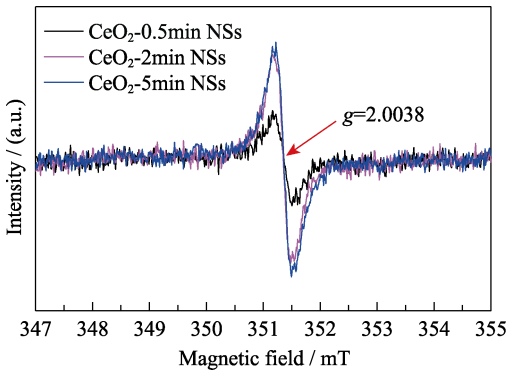

Fig. 6　EPR spectra of CeO_2 NSs

Reproducibility is a basic requirement for gas sensors to practical application. 500 μL/L CO at 450 ℃ was adopted to test reproducibility. In Fig. 7(b), it is found that the response of 7-time testing is stable without any decrease. It demonstrates that CeO_2-2min NSs possesses well reproducible ability in CO gas sensing.

Relationship between CO concentration and its response is important to determine real CO concentration in CO gas sensor applications. Different concentration of CO

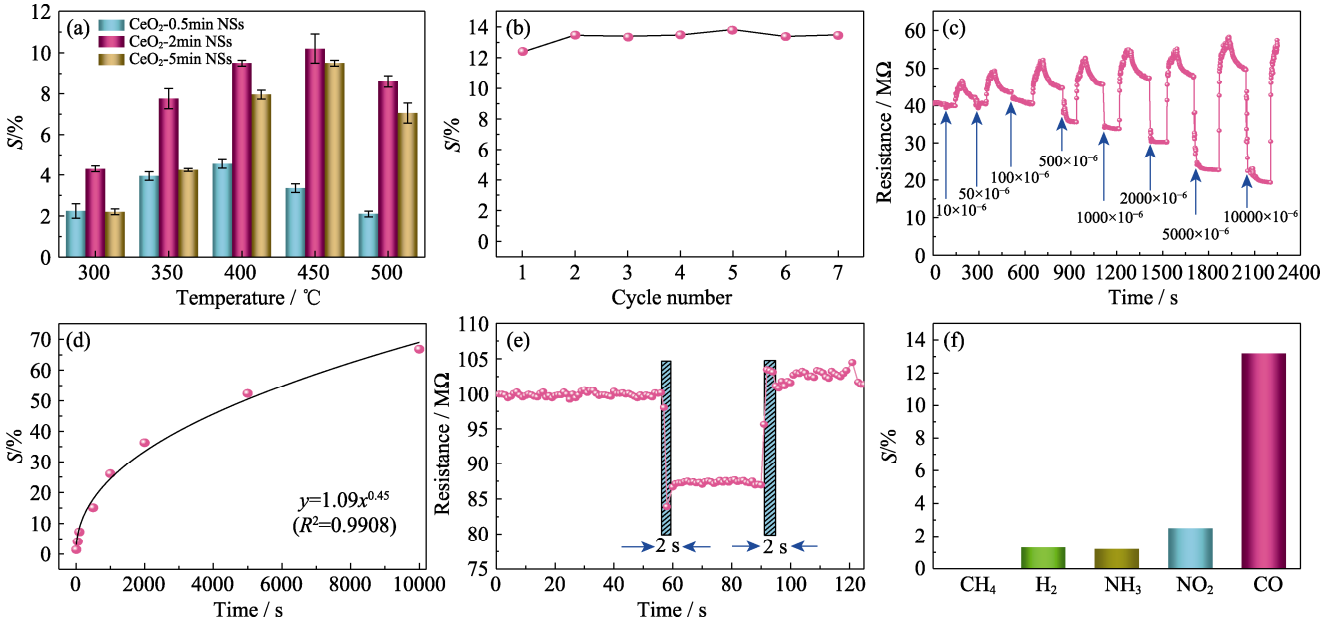

Fig. 7　Gas sensing properties of CeO_2 NSs

(a) Response of CeO_2 NSs at different temperatures from 300 ℃ to 500 ℃ with an interval of 50 ℃ towards 500 μL/L CO; (b) Response of CeO_2-2min NSs towards 500 μL/L CO at 450 ℃ for seven periods; (c) Transient response of CeO_2-2min NSs towards different concentration from 10 μL/L to 10000 μL/L at 450 ℃; (d) Fitting of CO concentration and its corresponding response; (e) Determination of response/recovery time of CeO_2-2min NSs towards 500 μL/L CO at 450 ℃; (f) Selectivity of CeO_2-2min NSs towards CH_4, H_2, NH_3, NO_2 and CO at 450 ℃

was subject to test at 450 ℃ as shown in Fig. 7(c). The highest concentration of the test is 10000 μL/L, and with the decrease of the concentration, the response also declines. Meanwhile, the lowest concentration tested is 10 μL/L with the response of 1.5%. Furthermore, the response and the concentration of CO (10–10000 μL/L) is fitted as shown in Fig. 7(d) and it keeps functional relationship of $y=1.09x^{0.45}$ with $R^2=0.9908$. It proves that CeO_2-2min NSs is a promising material in CO gas sensing with a wide range. In addition, it is impressive that the response/recovery time are ultrafast in the sensing procedure, which is expected for a gas sensor.

To investigate response/recovery time carefully, we chose a cycle of transient response in reproducibility test for further research. As can be seen in Fig. 7(e), the response and recovery time are both 2 s, which is very short in gas sensing. As discussed above, carriers on nanosheets move quickly because the morphology constraints its pathway in planes. In this case, electrons move in planes of CeO_2 nanosheets, which promises ultrafast response/recovery time. Therefore, it is reasonable to deem that CeO_2-2min NSs is advantageous in CO gas sensing. Moreover, recent progresses in CO gas sensing are summarized in Table 1, and it is concluded that CeO_2-2min NSs outperforms in response/recovery time.

Selectivity is a valuable index to evaluate gas sensor. We also studied the selectivity of CeO_2-2min NSs in gas sensing was studied as presented in Fig. 7(f). 500 μL/L of CH_4, H_2, NH_3, NO_2 and CO are subject to test, and it is found that the response of CO is much higher than that to other gases. Therefore, CeO_2-2min NSs is very promising in CO gas sensing.

In addition, it is noticed that humidity has obvious impact on CeO_2-2min NSs response (Fig. S2), namely high humidity for low response, which may be arisen from the water molecules occupy the active sites on CeO_2 NSs at high humidity. Besides, long-term stability of CeO_2-2min was also performed as shown in Fig. S3. Although the response has a small decrease in two weeks, long-term stability is improved by doping or coating in followup work.

2.3 Gas sensing mechanism

The gas sensing mechanism of CeO_2 NSs follows a surface charge model, which can be explained by the change of resistance in different target gases, as shown in Fig. 8[5,28]. In oxygen atmosphere (ambient air), oxygen molecules are adsorbed on the surface of the sensing materials by capturing free electrons, forming adsorbed oxygen anion species depended on the temperature[29-30]. In this study, when CeO_2 NSs are exposed to air, oxygen molecules are adsorbed on the surface trapping electrons from them, which forms depletion layer and an increased resistance. Subsequently, oxygen anions change as the sequence of O_2^-, O^- and O^{2-} along with the temperature rising. At last, when reducing gas CO is introduced, the CO gas molecules adsorb on the surface of CeO_2 NSs and then react with O^{2-} (the operating temperature is 450 ℃). The whole procedure may proceed as following equations:

$$O_{2(ads)} + e^- \rightarrow O_2^-{}_{(ads)} \quad (2)$$

$$O_2^-{}_{(ads)} + e^- \rightarrow 2O^-{}_{(ads)} \quad (3)$$

$$O^-{}_{(ads)} + e^- \rightarrow O^{2-}{}_{(ads)} \quad (4)$$

$$CO + O^{2-}{}_{(ads)} \rightarrow CO_2 + 2e^- \quad (5)$$

During this reaction, the release of electrons into the surface of CeO_2 NSs increases the concentration of carriers, leading to a thinner depletion layer as well as a decrease of resistance.

In this case, CeO_2-2min NSs possesses the largest part of O_V, which is the active site for facilitating oxygen adsorption and dissociation by providing unpaired electrons[13]. Besides, CeO_2-2min NSs holds largest pore diameter, which guarantees that CO molecules penetrate into the inside of sensing materials to touch more active sites[31]. Therefore, CeO_2-2min NSs deserves the highest response as discussed above. On the contrary, the small amount of as well as small pore diameters of O_V of CeO_2-0.5min NSs, which pays for a low response. In addition, nanosheets can constrain carriers to transport in

Table 1 Recent materials for in CO gas sensing

Material	Concentration/(μL·L^{-1})	Temperature/℃	Sensitivity	(Response/recovery time)/s	Ref.
Co_3O_4 nanostructures	5	100	2.4[a]	14/36	[23]
Pd/SnO_2	100	100	3.5[a]	60/150	[24]
TiO_2-CeO_2 mixed oxides	400	200	10.7[a]	32/45	[25]
SnO_2/MoO_2	100	RT	9.2%[b]	20/16	[1]
SnO_2-CeO_2 mixed oxides	500	430	190%[b]	26/30	[11]
Pd/SnO_2 nanowires	200	400	6.8[a]	5/40	[26]
ZnO nanorods	30	400	1.1[a]	46/27	[27]
Porous CeO_2 nanosheets	500	450	12.0%[b]	2/2	This work

a: the sensitivity is defined as $S=R_a/R_g$; b: the sensitivity is defined as $S=|R_a-R_g|/R_a\times100\%$

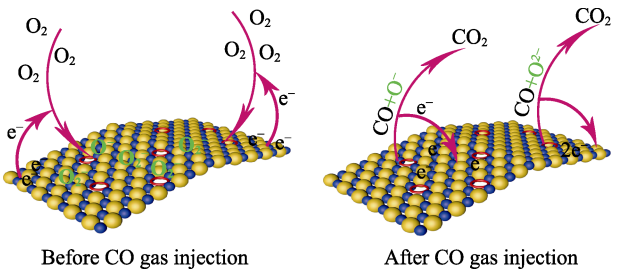

Fig. 8　Schematic illustration of CO gas sensing mechanism
Yellow spheres represent O atoms; Orange spheres represent Ce atoms; Red rings represent the position of oxygen vacancies

planes, which make carriers possess ultrafast mobility. On the other hand, oxygen vacancies can also increase mobility of carriers with easy movement between vacancies. These factors all contribute to ultrafast response/recovery time in this study.

3　Conclusion

In summary, CeO_2 NSs *via* flame annealing intermediate product $CeCO_3OH$ nanosheets was synthesized by hydrothermal method with different flame time. Wherein, CeO_2-2min NSs showed superb gas sensing performances. The response/recovery time were only 2 s/2 s, which was ultrafast in gas sensing field. In addition, CO concentration and its response kept well functional relationship at a wide detection range. Moreover, reproducibility and selectivity were also decent. The good performances are attributed to more oxygen vacancies and porous nanosheets morphology. As a result, this CeO_2 NSs is reliable to apply in CO gas sensing. Meanwhile, flame annealing provides a novel method to prepare nanomaterials with simplicity and low cost.

Supporting Materials

Supporting materials related to this article refer to https://doi.org/10.15541/jim20210142.

References:

[1] YANG Z, ZHANG D, WANG D. Carbon monoxide gas sensing properties of metal-organic frameworks-derived tin dioxide nanoparticles/molybdenum diselenide nanoflowers. *Sensors and Actuators B: Chemical*, 2019, **304:** 127369.

[2] BASU A K, CHAUHAN P S, AWASTHI M, *et al*. α-Fe_2O_3 loaded rGO nanosheets based fast response/recovery CO gas sensor at room temperature. *Applied Surface Science*, 2019, **465:** 56–66.

[3] WHO. WHO Air Quality Guidelines-Global Update 2005. World Health Organization, Copenhagen, 2006.

[4] YANG S, JIANG C, WEI S H. Gas sensing in 2D materials. *Applied Physics Reviews*, 2017, **4(2):** 021304.

[5] DEY A. Semiconductor metal oxide gas sensors: a review. *Materials Science and Engineering: B*, 2018, **229:** 206–217.

[6] MAHAJAN S, JAGTAP S. Metal-oxide semiconductors for carbon monoxide (CO) gas sensing: a review. *Applied Materials Today*, 2020, **18:** 100483.

[7] GOVARDHAN K, GRACE A N. Metal/Metal oxide doped semiconductor based metal oxide gas sensors-a review. *Sensor Letters*, 2016, **14:** 741–750.

[8] SUN C, LI H, CHEN L. Nanostructured ceria-based materials: synthesis, properties, and applications. *Energy & Environmental Science*, 2012, **5(9):** 8475–8505.

[9] LIU Y, LEI Y. Pt-CeO_2 nanofibers based high-frequency impedancemetric gas sensor for selective CO and C_3H_8 detection in high-temperature harsh environment. *Sensors and Actuators B: Chemical*, 2013, **188:** 1141–1147.

[10] MAJUMDER D, ROY S. Development of low-ppm CO sensors using pristine CeO_2 nanospheres with high surface area. *ACS Omega*, 2018, **3(4):** 4433–4440.

[11] DURRANI S M, AL-KUHAILI M F, BAKHTIARI I A, *et al*. Investigation of the carbon monoxide gas sensing characteristics of tin oxide mixed cerium oxide thin films. *Sensors (Basel)*, 2012, **12(3):** 2598–2609.

[12] LIU X, MA T, PINNA N, *et al.* Two-dimensional nanostructured materials for gas sensing. *Advanced Functional Materials*, 2017, **27(37):** 1702168.

[13] LIU F, WANG X, CHEN X, *et al.* Porous ZnO ultrathin nanosheets with high specific surface areas and abundant oxygen vacancies for acetylacetone gas sensing. *ACS Applied Materials Interfaces*, 2019, **11(27):** 24757–24763.

[14] MIAO J, CHEN C, MENG L, *et al.* Self-assembled monolayer of metal oxide nanosheet and structure and gas-sensing property relationship. *ACS Sensors*, 2019, **4(5):** 1279–1290.

[15] CHOI P G, IZU N, SHIRAHATA N, *et al.* SnO_2 nanosheets for selective alkene gas sensing. *ACS Applied Nano Materials*, 2019, **2(4):** 1820–1827.

[16] LI P, WANG B, QIN C, *et al.* Band-gap-tunable CeO_2 nanoparticles for room-temperature NH_3 gas sensors. *Ceramics International*, 2020, **46(11):** 19232–19240.

[17] LI P, WANG B, LI W, *et al.* Effect of annealing atmosphere with different oxygen concentration on CO gas sensing performances for CeO_2 nanoparticles. *Materials Letters*, 2021, **284:** 129000.

[18] SAMERJAI T, CHANNEI D, KHANTA C, *et al.* Flame-spray-made ZnInO alloyed nanoparticles for NO_2 gas sensing. *Journal of Alloys and Compounds*, 2016, **680:** 711–721.

[19] YUAN H, ALJNEIBI S, YUAN J, *et al.* ZnO nanosheets abundant in oxygen vacancies derived from metal-organic frameworks for ppb-level gas sensing. *Advanced Materials*, 2019, **31(11):** e1807161.

[20] ZHAO H, DONG Y, JIANG P, *et al.* Highly dispersed CeO_2 on TiO_2 nanotube: a synergistic nanocomposite with superior peroxidase-like activity. *ACS Applied Materials Interfaces*, 2015, **7(12):** 6451–6461.

[21] DENG C, HUANG Q, ZHU X, *et al.* The influence of Mn-doped CeO_2 on the activity of CuO/CeO_2 in CO oxidation and NO+CO model reaction. *Applied Surface Science*, 2016, **389:** 1033–1049.

[22] YAO L, LI Y, RAN Y, *et al.* Construction of novel Pd-SnO_2 composite nanoporous structure as a high-response sensor for methane gas. *Journal of Alloys and Compounds*, 2020, **826:** 154063.

[23] BUSACCA C, DONATO A, LO FARO M, *et al.* CO gas sensing performance of electrospun Co_3O_4 nanostructures at low operating temperature. *Sensors and Actuators B: Chemical*, 2020, **303:** 127193.

[24] WANG Q, WANG C, SUN H, *et al.* Microwave assisted synthesis of hierarchical Pd/SnO_2 nanostructures for CO gas sensor. *Sensors and Actuators B: Chemical*, 2016, **222:** 257–263.

[25] MOHAMMADI M R, FRAY D J. Nanostructured TiO_2-CeO_2 mixed oxides by an aqueous Sol-Gel process: effect of Ce:Ti molar

ratio on physical and sensing properties. *Sensors and Actuators B: Chemical*, 2010, **150(2):** 631–640.

[26] TRUNG DO D, HOA N D, TONG P V, *et al.* Effective decoration of Pd nanoparticles on the surface of SnO_2 nanowires for enhancement of CO gas-sensing performance. *Journal of Hazard Materials*, 2014, **265:** 124–132.

[27] KHOANG N D, HONG H S, TRUNG D D, *et al.* On-chip growth of wafer-scale planar-type ZnO nanorod sensors for effective detection of CO gas. *Sensors and Actuators B: Chemical*, 2013, **181:** 529–536.

[28] QIN C, WANG B, WU N, *et al.* Metal-organic frameworks derived porous Co_3O_4 dodecahedeons with abundant active Co^{3+} for ppb-level CO gas sensing. *Applied Surface Science*, 2020, **506:** 144900.

[29] XU J M, CHENG J P. The advances of Co_3O_4 as gas sensing materials: a review. *Journal of Alloys and Compounds*, 2016, **686:** 753–768.

[30] YAN F, SHEN G, YANG X, *et al.* Low operating temperature and highly selective NH_3 chemiresistive gas sensors based on Ag_3PO_4 semiconductor. *Applied Surface Science*, 2019, **479:** 1141–1147.

[31] WANG Z, YU R. Hollow micro/nanostructured ceria-based materials: synthetic strategies and versatile applications. *Advanced Materials*, 2019, **31(38):** e1800592.

基于火焰退火多孔 CeO_2 纳米片的环境监测用超快 CO 气体传感器

李鹏鹏, 王 兵, 王应德

(国防科技大学 空天科学学院, 新型陶瓷纤维及其复合材料重点实验室, 长沙 410073)

摘 要: CO 作为一种高毒性的气体，既是污染空气的元凶之一，长时间吸入也会对人体造成极大的伤害，甚至致死。如何实现 CO 的快速监测是传感领域面临的重要挑战。CO 监测对保护人类健康和环境来说是一项必要的工作。在该研究中, 多孔 CeO_2 纳米片(CeO_2 NSs)通过火焰退火用简单水热法合成的中间产物 $CeOHCO_3$ 纳米片而得到。通过控制火焰退火时间, 可将氧空位引入到 CeO_2 纳米片中。结果表明, 退火 2 min 得到的 CeO_2 纳米片(CeO_2-2min NSs)对 CO 气体表现出优异的重复性和选择性。尤其是, CeO_2-2min NSs 在 450 ℃对 500 μL/L CO 的相应/恢复时间极快(2 s/2 s), 在宽范围内(10~10000 μL/L) CO 浓度与响应值之间存在良好的函数关系。CeO_2-2min NSs 优秀的气敏性能可归因于多孔二维结构高的比表面积和晶体内丰富的氧空位。这项工作对设计检测宽范围气体的快响应气体传感器提供了借鉴。

关 键 词: 火焰退火; 多孔 CeO_2 纳米片; 氧空位; 气体传感器; 宽范围

中图分类号: TQ174 **文献标志码**: A

Supporting materials:

Ultrafast CO Sensor Based on Flame-annealed Porous CeO_2 Nanosheets for Environmental Application

LI Pengpeng, WANG Bing, WANG Yingde

(Science and Technology on Advanced Ceramic Fibers and Composites Laboratory, College of Aerospace Science and Engineering, National University of Defense Technology, Changsha 410073, China)

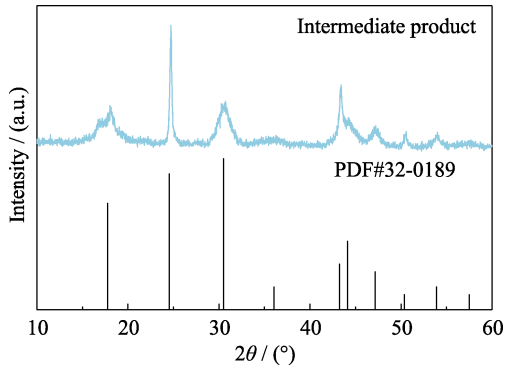

Fig. S1　XRD pattern of the intermediate product

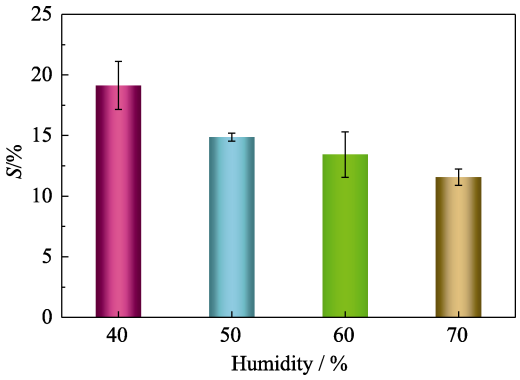

Fig. S2　Response of CeO_2-2min NSs towards 500 μL/L CO at 450 ℃ under different humidities

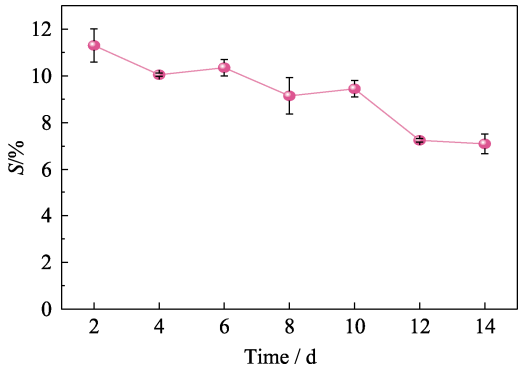

Fig. S3　Long-term stability of CeO_2-2min NSs towards 500 μL/L CO at 450 ℃ for two weeks

Table S1　Percentage of each element species to the whole element content

	O_S/%	O_V/%	Ce^{3+}/%	Ce^{3+}/Ce^{4+}
CeO_2-0.5min NSs	19.0	40.0	26.3	0.357
CeO_2-2min NSs	14.8	43.2	28.6	0.401
CeO_2-5min NSs	15.1	42.7	23.8	0.312

Table S2　Summary of surface area and pore volume of CeO_2 NSs

	Surface area/($m^2 \cdot g^{-1}$)	Pore volume/ ($cm^3 \cdot g^{-1}$)	Average pore diameter/nm
CeO_2-0.5min NSs	73.344	0.172	10.1
CeO_2-2min NSs	46.804	0.181	15.5
CeO_2-5min NSs	40.836	0.163	15.8